AIP Journal of Applied Physics

Study of the oxygen vacancies changes in SnO2 polycrystalline thick films using impedance and photoemission spectroscopies

F. Schipani, M. A. Ponce, E. Joanni, F. J. Williams, and C. M. Aldao

Citation: Journal of Applied Physics **116**, 194502 (2014); doi: 10.1063/1.4902150

View online: http://dx.doi.org/10.1063/1.4902150

View Table of Contents: http://scitation.aip.org/content/aip/journal/jap/116/19?ver=pdfcov

Published by the AIP Publishing

Study of the oxygen vacancies changes in SnO_2 polycrystalline thick films using impedance and photoemission spectroscopies

F. Schipani,[1] M. A. Ponce,[1] E. Joanni,[2] F. J. Williams,[3] and C. M. Aldao[1,a)]
[1]*Institute of Materials Science and Technology (INTEMA), University of Mar del Plata and National Research Council (CONICET), Juan B. Justo 4302, B7608FDQ Mar del Plata, Argentina*
[2]*CTI Renato Archer, Rodovia D. Pedro I (SP-65) Km 143.6, CEP: 13069-901, Campinas, São Paulo, Brasil*
[3]*Departamento de Quimica Inorganica, Analitica y Quimica Fisica and INQUIMAE, Facultad de Ciencias Exactas y Naturales, Universidad de Buenos Aires and CONICET. Pab. 2, piso 3, C1428EHA Buenos Aires, Argentina*

(Received 9 September 2014; accepted 7 November 2014; published online 18 November 2014)

Changes in the concentration of oxygen vacancies within the grains of polycrystalline SnO_2, due to different atmosphere exposures, were detected using impedance and photoemission spectroscopies. From measured capacitance values, variations of the potential barrier widths could be determined. It is shown that under the presence of an oxygen rich atmosphere, at relatively low temperature, the width of intergranular potential barriers increase to the point that grains become completely depleted of carriers. With subsequent exposure to vacuum, capacitance adopts a higher value, indicative of intergranular barriers and quasi-neutral regions at the center of the grains. X-ray and ultraviolet photoemission spectroscopy measurements showed that SnO_2 samples treated in oxidizing or reducing environments have similar barrier heights and different work functions. Results are especially relevant in the study of mechanisms responsible for metal oxide gas sensing. © *2014 AIP Publishing LLC*. [http://dx.doi.org/10.1063/1.4902150]

I. INTRODUCTION

Semiconducting metal oxide sensors, like SnO_2, present characteristics such as sensitivity, long-term stability, robustness, and low price, which make them extremely valuable in the field of gas sensing. Gas sensors based on oxide semiconductors detect gases as electrical impedance changes upon gas adsorption and diffusion in a porous layer.[1–3] Consequently, the ceramic gas sensor performance depends on the porous microstructure, and on the surface reactivity with the gas. Then, as the sensitivity of these sensors depends on the film microstructure and on the substrates shape, the fabrication process is crucial in improving the sensors response.

It is widely accepted that barriers formed between particles or grains have a Schottky-type nature and that they govern the electrical behavior of the sensor. Adsorption of gaseous species at the grain boundaries can induce changes in the barriers heights and in the donor concentrations. Many oxide semiconductors have a large number of oxygen vacancies conferring their n-character. Chemisorbed oxygen species (O^{-2} and O^{-}) act as electron acceptors and lead to the formation of a depletion layer extending into the grains forming surface barriers.[4] These surface barriers play a key role as they control electron transfer between grains, affecting the overall resistance.[5–8]

We focus here on oxygen vacancies as they directly affect conductivity and therefore the film gas detection ability. In fact, oxygen vacancies, being the main dopant in tin oxide and other semiconducting oxides, are also relevant in other related issues. For example, it has been argued that the degradation in metal oxide varistors is controlled by a defect electro-migration process of defects.[9] Degradation phenomena can appear under continuous, alternating, or pulses of voltage usually combined with thermal treatments.[10,11] Also, it has been shown that degraded ZnO varistors can recover their properties under an oxygen atmosphere.[12] These type of experiments can be explained as the result of the deformation of Schottky barriers present in the grain boundaries in which oxygen vacancies play a central role.[13–18]

In this work, thick films of SnO_2 were made using the screen-printing method onto alumina substrates on which electrodes with an interdigitated shape were deposited by sputtering. Impedance and photoelectron spectroscopies were used to characterize the intergranular potential barriers. Results indicate that the oxygen vacancy density varies within the grains as films are exposed to different atmospheres at relatively low temperatures. A detailed study of the capacitance measurements indicates that under the presence of an oxygen rich atmosphere, the dopant density drops to the point that barriers overlap and then grains become completely depleted of carriers. X-ray and UV Photoelectron Spectroscopy (XPS and UPS) measurements allow us to determine changes in barrier heights and in work functions of samples with different gas pre-treatments.

II. EXPERIMENTAL

Thick, porous film samples were made by painting onto insulating 96% dense alumina substrates on which electrodes with an interdigitated shape were deposited by sputtering. Alumina substrates were cleaned with acetone and isopropyl alcohol, blown with dry nitrogen, and placed in a sputtering chamber. After pumping the chamber to its base pressure

a)Author to whom correspondence should be addressed. Electronic mail: cmaldao@fi.mdp.edu.ar

(10^{-6} mbar), an adhesion layer consisting of 25 nm of titanium was deposited. Without breaking vacuum, a platinum film 200 nm thick was then deposited over the Ti layer. For defining the electrodes, the substrates with the metal films were placed in a home-built micromachining system consisting of three translation stages and a 20 W, frequency tripled Nd:YVO4 laser (lambda = 355 nm). The interelectrode distance was 20 μm. Fig. 1(a) shows a picture of the used type of substrate and Fig. 1(b), a detail of the interelectrode.

Commercial high-purity SnO_2 (Aldrich 99.99%, medium particle size 0.4 μm) was ground until a medium particle size of 0.130 μm was obtained as determined using the intersection method from SEM images. To image the tin oxide surfaces, a JEOL JSM 6460-S scanning electron microscope was employed. In Fig. 2, we present a micrograph of the film showing a porous structure as required for sensors. The grain size is crucial for the electrical properties, as previously discussed in detail. In order to evaporate the binder, the resulting powder was heated up to 380 °C and maintained at this temperature for 1 h, using a heating rate of 1 °C/min. Later, the powder was cooled to 25 °C and a paste was prepared with an organic binder (glycerol). The used solid/organic binder ratio was 1/2, and no dopants were added.

After painting, samples were thermally treated for 1 h in air at 100 °C. This treatment was performed in order to evaporate the organic binder and to improve the adhesion of the films on the alumina substrate. Later, samples were thermally treated up to 380 °C using a heating rate of 1 °C/min and exposed to an air atmosphere at 380 °C during 1 h. After thermal treatment, the film was cooled down to 25 °C. Finally, some of the samples were kept at 380 °C for 4 h in a N_2 atmosphere with 5% H_2. Samples were labeled S_{O2} (samples only exposed to dry air) and S_{H2} (samples exposed to hydrogen). Samples were placed in the measuring cell, which was then evacuated. The average thickness of the film

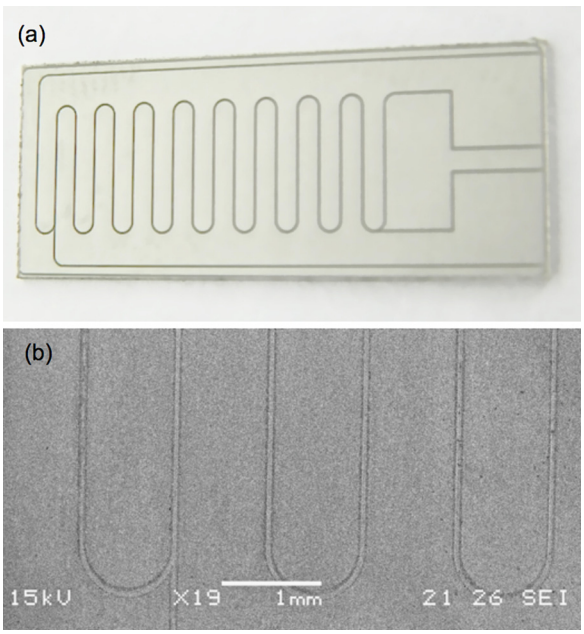

FIG. 1. (a) Substrate of 20 mm length and 10 mm wide used in the experiments. (b) Detail of the interelectrode of 20 μm.

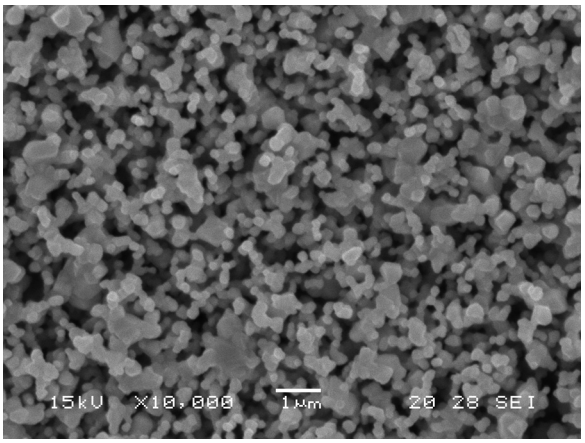

FIG. 2. SEM micrograph of the film showing a porous structure with an average grain size of 0.130 μm as determined using the intersection method.

was 0.105 mm as shown in Fig. 3 in which a micrograph of the cross section is presented.

An X-ray powder diffraction (XRD) analysis was carried out with a Philips (PW1830) diffraction system employing CuKα radiation at 40 kV and 40 mA, Fig. 4. Samples were scanned between 20° and 80° with a step size of 0.01°. The XRD data were analyzed using the X'Pert PRO HighScore software. Our samples showed a single phase corresponding to tin oxide reference code 01-072-1147 of the International Centre for Diffraction Data (ICCD) (1998) Powder diffraction file database, Newtown Square (USA).

The resistance was measured, while raising and then decreasing the temperature from room temperature up to 350 °C at a rate of ~1 °C/min with the sample kept in vacuum. Measurements were made after reaching steady state at different temperatures of the experiment range. An Agilent

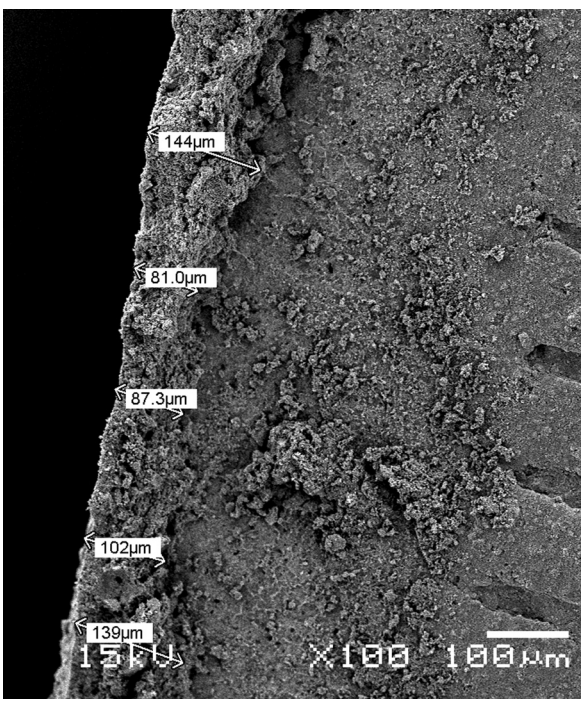

FIG. 3. Micrograph of the cross section of the film that presents an average thickness of 0.105 mm.

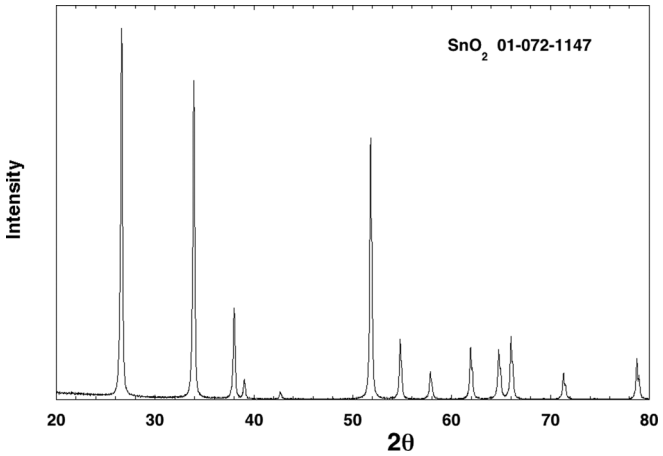

FIG. 4. High quality X-ray diffraction pattern in the range 20°–80° (2θ). A tin oxide tetragonal crystalline system is only observed in the powder used in our samples.

3440 A multimeter was used for the electrical conductance measurements. Finally, capacitance *vs.* frequency, measurements were carried out with a Hewlett Packard impedance analyzer model 4184 A with samples exposed to vacuum at different temperatures.

XPS and UPS measurements were performed under ultra high vacuum conditions (base pressure $< 5 \times 10^{-10}$ mbar) in a SPECS spectrometer system equipped with a 150 mm mean radius hemispherical electron energy analyzer and a nine channeltron detector. XPS spectra were acquired at a constant pass energy of 20 eV using an un-monochromated MgKα (1253.6 eV) source operated at 12.5 kV and 20 mA and a detection angle of 30° with respect to the sample normal on grounded conducting substrates. The binding energies quoted are referred to the Au $4f_{7/2}$ emission at 84.0 eV. UPS spectra were acquired using a He I radiation source (21.2 eV) operated at 100 mA with normal detection at constant pass energy of 2 eV. Samples were biased −8 V in order to resolve the secondary electron cutoff in the UPS spectra. Work function values were determined from the width of the UPS spectra as discussed below.

III. RESULTS AND DISCUSSIONS

As we have proposed previously, at temperatures greater than ~200 °C changes in conductivity could be attributed to a reduction in donor concentration implying oxygen diffusion into the grains with the consequent annihilation of oxygen vacancies. Conversely, if oxygen diffuses out of the grains, vacancies are generated. On the other hand, Electron Spin Resonance measurements indicate that adsorbed oxygen transfers electrons from the grains to the chemisorbed oxygen.[19,20] Consistently, the relevant reactions from the gas phase to the bulk of the grain for oxygen have been proposed to be[19]

$$O_{2(gas)} \leftrightarrow O_{2(ads)} \leftrightarrow O^{-}_{ads} \leftrightarrow O^{-2}_{ads} \leftrightarrow O^{-2}_{\text{int}} \leftrightarrow O^{-2}_{latt}, \quad (1)$$

where $O_{2(gas)}$ refers to oxygen in the gas environment, $O_{2(adss)}$ to an oxygen molecule adsorbed at the grain surfaces, $O^{-}{}_{ads}$ and $O^{-2}{}_{ads}$ to singly and doubly ionized monatomic oxygen at the grain surface, $O^{-2}{}_{int}$ to interstitial oxygen, and $O^{-2}{}_{latt}$ to oxygen at the tin oxide lattice. In the last part of Eq. (1), interstitial oxygen migrates from the surface to the bulk annihilating oxygen vacancies, V_O^{++}, *i.e.*

$$V_O^{++} + O^{-2}_{\text{int}} \leftrightarrow O_{latt}. \quad (2)$$

Therefore, exposing the SnO_2 sample to an oxygen rich atmosphere at high enough T results in a decrease in V_O^{++}. On the other hand, under vacuum V_O^{++} is expected to increase. The donor density, at which grains become completely depleted, due to their small size, can be relatively high. Assuming a spherical grain, this takes place when

$$V_s = \frac{eN_dR^2}{6\varepsilon_0\varepsilon_r}, \quad (3)$$

where V_s is the band bending, R is the grain radius, N_d is the dopant concentration, e is the electron charge, ε_0 is the vacuum permittivity, and ε_r is the relative permittivity. In our case, we can estimate that complete depletion occurs for $N_d \leq 7 \times 10^{23}$ m^{-3}.

The presence of undesirable contaminants was checked with X-ray photoemission spectroscopy (XPS). Figure 5 shows XPS spectra corresponding to the sample oxygen before (a) and after (b) thermally treated up to 380 °C in air. We chose this temperature because at higher temperatures, the films lose adhesion. Anyway, this temperature is enough to end up with a clean surface. Indeed, broad scans after the treatment show the presence of only Sn and O related peaks with no detectable amounts of any contaminants. Conversely, note the presence of the C 1 s signal at approximately 285 eV before the treatment.

By means of XPS core level analysis, comparative values of the interface Fermi level position in the gap can be determined as it is directly related to the XPS peak binding energy position. This can be accomplished using core levels peaks. In Fig. 6, we present results for O 1 s showing a

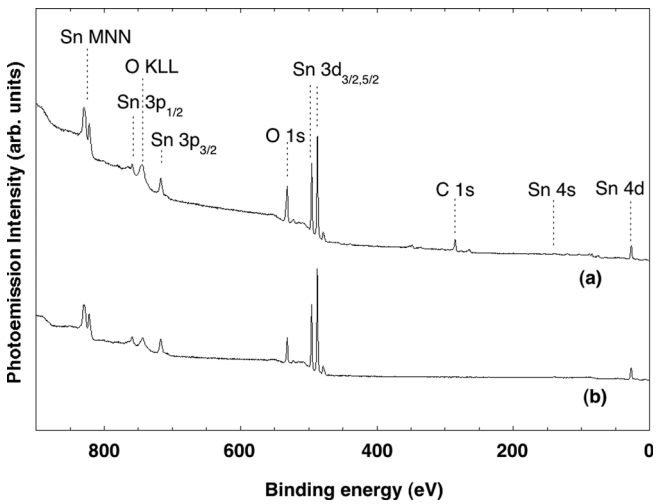

FIG. 5. (a) XPS broad scans for sample thermally treated for 1 h in air at 100 °C and (b) after thermally treated up to 380 °C using a heating rate of 1 °C/min and exposed to an air atmosphere at 380 °C during 1 h. Note that in spectrum (b), only Sn and O related XPS peaks are observed; while in (a), an important amount of C is detected.

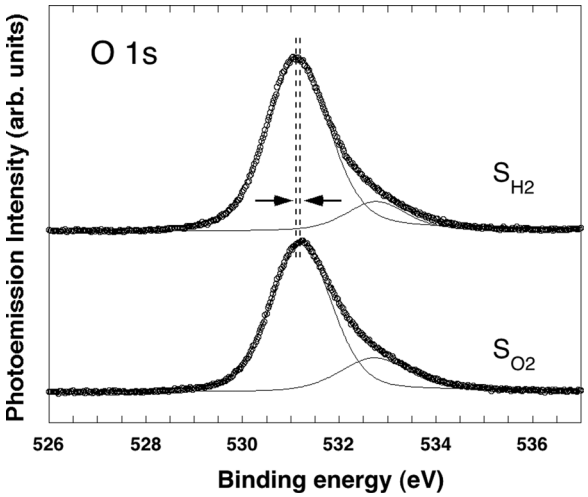

FIG. 6. O 1s core level energy distribution curves for the S_{H2} and the S_{O2} samples. Similar binding energy indicates that barrier heights do not differ considerably. The shoulder peak is 25% of the main peak in the S_{O2} sample and 14% of the main peak in the S_{H2} sample.

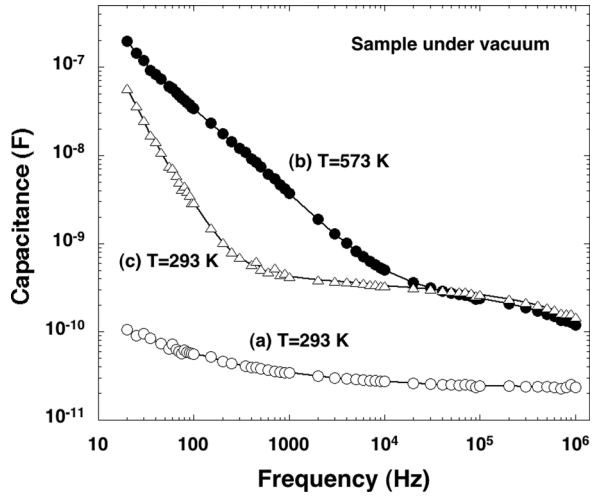

FIG. 7. Total capacitances vs. frequency during three stages of a thermal treatment carried out under vacuum. (a) corresponds to the sample initially at room temperature, (b) at T = 573 K, and (c) after cooling back to room temperature.

Schottky barrier difference of 0.07 eV with a slightly higher barrier for the S_{H2} sample, confirming our previous findings.[21] These results indicate that, regardless of the sample treatment, which leads to very different conductivities, surfaces under vacuum at room temperature present the same Schottky barrier height.

The O 1 s XPS signal of the films was fitted with two peaks located at 531.2 and 532.7 for the S_{O2} sample, 0.07 eV less for the S_{H2} sample. The high intense peak can be assigned to the O 1 s core level of the oxygen anions in the SnO_2. The shoulder peak has been proposed to be due to defect sites within the oxide crystal, chemisorbed oxygen, hydroxide species, or carbonaceous compounds.[22,23] This last option seems not possible, as carbon is not detected in the XPS spectrum. Hydroxide species should increase after treating the sample with hydrogen. However, the shoulder peak reduces from 25%, for the S_{O2} sample, to 14% of the intense peak, for the S_{H2} sample. It is known that polycrystalline materials present an interfacial component at the grain boundaries or at their surfaces. It has been proposed to have several atomic layers in which atoms do not keep the exact position corresponding to the crystal structure. Thus, we are prone to assign the shoulder peak to nonstoichiometries and disorder present at the grains surfaces due to oxygen vacancies and the surface itself. The action of hydrogen, then, would be to eliminate some of the unstable oxygen at or close to the surface responsible for the shoulder peak.

Figure 7 shows the total capacitances vs. frequency during three stages of a thermal treatment carried out under vacuum for the sample S_{O2}. In order to analyze the film capacitance behavior, it is necessary to consider the shape of the electrodes. According to the geometry of our sensors, the electrical capacitance can be related to that of semi-infinite electrodes, coplanar with a gap separating them[24]

$$C_0 = \frac{2\varepsilon_0\varepsilon_r}{\pi} l.\ln\left[\left(1+\frac{w}{a}\right)+\sqrt{\left(1+\frac{w}{a}\right)^2-1}\right], \quad (4)$$

where w is the width of the platinum interdigitated electrodes, $2a$ is the width of the inter-electrode pathway and, l is the length of the electrode (See Fig. 8). For the dimensions of our setup $w = 0.5$ mm, $l = 11$ cm, $a = 10\ \mu$m, with Eq. (4), we can calculate that C_0 is 2.88 pF for $\varepsilon_r = 1$.

Experimentally, we found that the capacitance before the incorporation of the sensor film for 1 MHz, C_1, is 12 pF. We have to consider that we have two capacitors in parallel, as on one side of the electrodes, there is air, with an associated capacitance C_{air}, and, on the other, the alumina substrate. Thus, the total capacitance C_1 is the sum of both sides' contributions.

Due to the symmetry of the arrange, we can write

$$C_{air} = C_0/2. \quad (5)$$

The contribution to the total capacitance due to the alumina of thick b_{alum}, can be expressed, as a good approximation[25]

$$C_{alum} = \frac{\varepsilon_0\varepsilon_{alum}}{\pi} l.\left[\sinh^{-1}(b_{alum}/a)+0.234\right], \quad (6)$$

where ε_{alum} is the alumina relative permittivity and the measured value of the alumina thickness is $b_{alum} = 0.41$ mm. Using Eq. (6) and correcting for the electrode width,[25] we could determine that $C_{alum}/\varepsilon_{alum} \approx 1.41$ pF. This value would

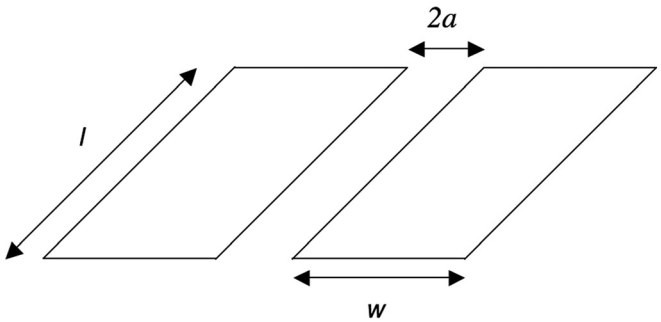

FIG. 8. Geometrical configuration of coplanar band electrodes.

be 1.44 pF for an infinitely thick alumina substrate implying that the contribution of the air beyond the alumina substrate is $C_a = 0.03$ pF.

Experimentally, we found that the capacitance after the incorporation of the sensor film, C_2, was 23.5 pF, value measured for 1 MHz [curve (a) of Fig. 7]. The contribution to the total capacitance due to the film of thick b_{film}, can be expressed, as a good approximation, as done before for the alumina side contribution

$$C_{film} = \frac{\varepsilon_0 \varepsilon_{film}}{\pi} l. \left[\sinh^{-1}\left(b_{film}/a\right) + 0.234 \right], \qquad (7)$$

where ε_{film} is the film relative permittivity and the measured value of the film thickness is $b_{film} = 0.105$ mm. With Eq. (7), we determined that $C_{film}/\varepsilon_{film} = 1.018$ pF, the correction for the electrode width is negligible in this case. As above, this value would be 1.44 pF for an infinitely thick film implying that the contribution of the air beyond the film is $C_b = 0.42$ pF.

First, the measured capacitance C_1, without the sensor film, can be expressed as

$$C_1 = C_{air} + C_{alum} + C_a. \qquad (8)$$

Thus, we can determine $C_{alum} = 10.53$ pF and then the alumina permittivity $\varepsilon_{alum} = 7.5$, value consistent with those reported in the literature.[26]

Second, the measured capacitance C_2, with the sensor film, can be expressed as

$$C_2 = C_{alum} + C_{film} + C_a + C_b. \qquad (9)$$

With Eq. (9), we can determine $C_{film} = 12.52$ pF and then the film permittivity $\varepsilon_{film} = 12.3$. This value represents an effective permittivity consistent with the values 9.6 and 13.5 for the parallel and perpendicular values of the permittivity, ε_1 and ε_2, to the regularly named c-axis in rutile.[27] Following Ref. 28, the effective permittivity for the given values of ε_1 and ε_2 can be calculated and results 12.4. Note that the found effective dielectric constants validate the performed calculations and the value found for the film permittivity indicates that grains are completely depleted of electrons.

Figure 9 shows a temperature cycle for a sample under vacuum in which the temperature was raised up to 295 °C and then back to room temperature. These results cannot be explained within the frame of a thermionic mechanism for conduction. With heating, the conductivity starts increasing with a slope corresponding to activation energy of 0.37 eV and then, above 150 °C, the slope reduces to 0.18 eV. We could assume that oxygen desorbs as the temperature is increased and then the activation energy would decrease with T. However, with a reducing barrier height, the conductivity should increase faster than at low temperatures, as a low activation energy facilitates conduction. On the other hand, we could assume that the activation energy increases with T. This could be due to the adsorbed oxygen being in the form of O_2^- below 150 °C and of O^- or O^{2-} above this temperature.[27] However, after cooling down, the conductivity adopts a much larger value than at the beginning of the cycle, result that is incompatible with a higher barrier.

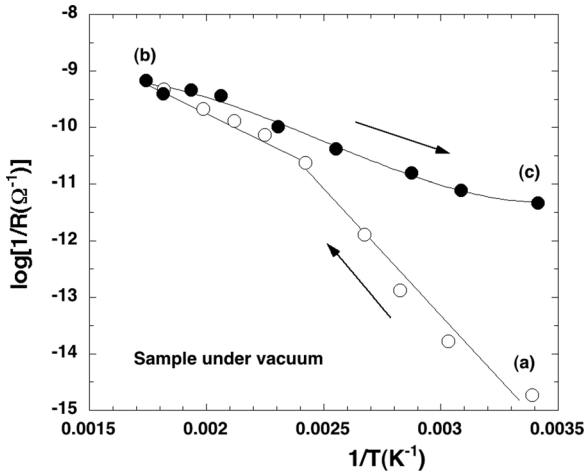

FIG. 9. Conductance in temperature cycling experiments. Temperature was raised up to 295 °C and then back to room temperature. After cooling down, the conductivity adopts a much larger value than at the beginning of the cycle. Lines are a guide to the eye.

As already mentioned, it has long been recognized that Schottky barriers at grain surfaces determine the conductance of this type of films. Consequently, adsorption of different gases is accompanied by changes in these barriers, which affects electron transport between grains and thus the resistance of the device changes. Conduction mechanisms have been interpreted in analogy to those in metal-semiconductor contact diodes. Accordingly, the electrical properties of polycrystalline semiconductors are usually described with a simple one-dimensional model representing the interface between two grains. It is regularly considered that a thermionic mechanism is responsible for the sample conductivity. However, it has been pointed out that a thermionic-field emission or tunneling contributions are unavoidable for the usual barriers characteristics.[29] In short, two models have been mostly used in the literature to rationalize electron conduction in polycrystalline SnO_2: an activated thermionic mechanism that depends only on intergranular barrier heights, and an electron tunneling mechanism that depends both on intergranular barrier heights and widths.

We propose that the present findings can be the consequence of oxygen intragranular diffusion, which takes place when heating the samples to a high enough temperature, affecting oxygen vacancies concentration and, then, Schottky barrier widths.[14,30] The thermionic contribution to conductivity would not be strongly modified as long as barrier heights remain constant, as XPS results indicate, but the thermionic-field emission contribution would be especially affected as tunneling depends on both height and width of the barriers. As temperature is raised, oxygen diffuses out of the sample increasing the donor density, because oxygen vacancies are the dominating donor. Thus, tunneling is favored and, after cooling down, the sample presents a much higher conductivity. In a low-doped sample, grains can be completely depleted and, for a doping high enough, grains can have a bulk region in their centers. Thus, the slope change in conductivity at about 140 °C is an indication that oxygen diffusion led to a doping that narrowed the space charge regions to the point at which grains are not completely depleted.[15,18,31]

Results of Fig. 7 represent strong evidence in favor of the above interpretation. Curve (a) corresponds to the sample after being exposed to an atmosphere rich in oxygen and the measured capacitance is that expected for bulk tin oxide, as calculated above. This implies that grains are completely depleted of carriers. Curve (b) of Fig. 7 is the capacitance as a function of frequency for the sample at T = 573 K that corresponds to point (b) in Fig. 9. At this stage of the heating cycle, from conductance behavior, we proposed that oxygen diffusion from the bulk of the grains to the intergrains took place. This is consistent with a higher dopant concentration due to vacancy formation, which reflects in a larger capacitance as the grains present barriers narrow enough to be non overlapped, *i.e.*, they have quasi-neutral regions at their centers. On the other hand, deep traps effects are observed, which, as expected, influence the measured capacitance up to a relatively high frequency at this temperature. To facilitate the comprehension of capacitance changes after oxygen vacancy increase, conduction band diagrams with overlapped potential barriers and with non-overlapped potential barriers are shown in Fig. 10.

After heating, the measured capacitance is not so simple to analyze quantitatively as before, case (a), when grains were completely depleted of carriers. Now, electrically, the film consists in a complex network of resistors and capacitors. In addition to the effect of traps, the observed curvature in the capacitance vs. frequency dependence at high frequencies has been shown to be the effect of the random character of the network.[32] However, at enough high frequency, one can consider that the impedance of the capacitors is much lower than that of the resistors and then we end up with a random capacitor network. In the following analysis, we will assume a final value of ≈100 pF.

For non-overlapped potential barriers, the capacitance of an intergrain is that of two Schottky barriers in series. In a 1D approximation, the resulting capacitance, C'_{film}, related to that corresponding to a sample with overlapped barriers, C_{film}, can be expressed as

$$\frac{C'_{film}}{C_{film}} = \frac{d}{2\Lambda}, \tag{10}$$

where d is the grain size and Λ is the depletion layer width. The ratio between the film capacitances before and after the heating cycle is ≈7.1, using Eq. (9). This change can be interpreted with Eq. (10) as depletion widths become narrower than the grain radius, consequence of a higher doping.

With Eq. (10), the depletion width can be determined to be ≈9.1 nm. We have recently reported a barrier height of 0.69 eV for this type of samples.[21] Given this barrier height, doping after the heating should be $N_d \approx 1.1 \times 10^{25}\ m^{-3}$. This doping value is similar to that deduced from the measured conductivity reported in Ref. 21, which is remarkable considering all the approximations involved in our calculations. Note that the change in capacitance cannot be due to a barrier lowering, as this would imply a change in conductivity not compatible with the conductivity results of Fig. 9.

Figure 11 shows the valence band density of states obtained with UPS for the S_{O2} and S_{H2} samples. Three regions can be resolved. The main feature at low binding energy, at about 5 eV, is mainly of O 2p character, while the region at about 7 eV corresponds to the hybridization of Sn 5p with O 2p. Also, around 3 eV, gap states are observed as shown in the amplified spectrum. Samples of different preparations show similar valence bands with practically the same valence band maximum indicating the same band bending in agreement with the results of Fig. 6.

The work function, WF, is the energy needed to extract an electron from a solid, *i.e.*, the difference between the vacuum level and the Fermi level, E_{vac}-E_F. In a semiconductor, the work function can be modified by changing the position of the conduction band bottom respect the Fermi level

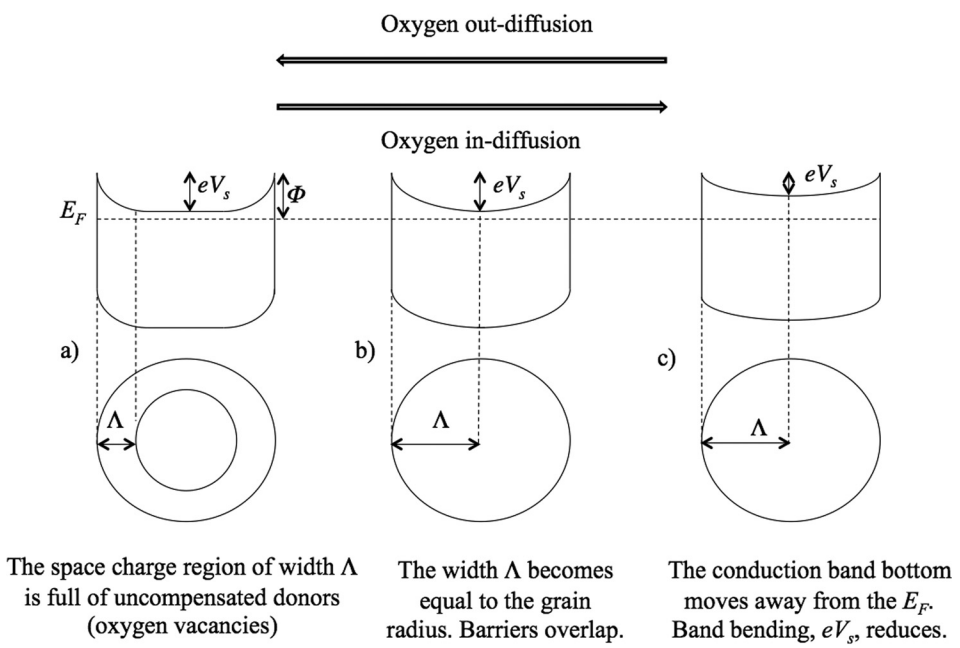

FIG. 10. Band diagrams showing the effect of increasing the doping in a semiconductor grain. When depletion layers do not overlap, there is a bulk region at the center of the grain with no net charge in which donors are compensated (a). As doping decreases, due to oxygen diffusion into the grain, the space charge region increases to the point at which the grain is completely depleted of electrons (b). Further decreasing of doping raises the bottom of the conduction band within the grain.

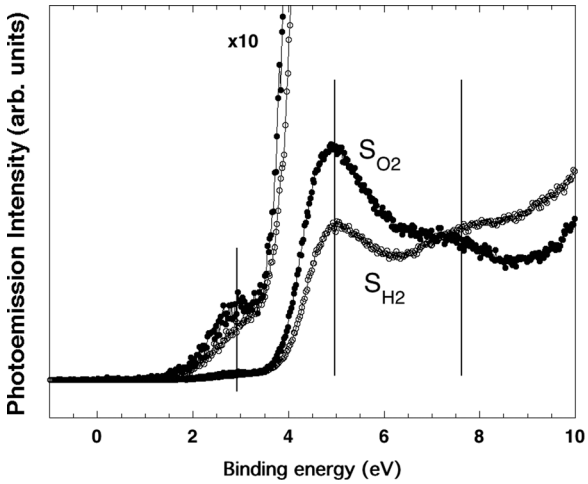

FIG. 11. UPS spectra for the S_{H2} and S_{O2} samples. Long lines indicate contributions of O 2p, at about 5 eV, and of Sn 5p with O 2p hybridization, around 7 eV. Gap states are observed around 3 eV, short line, as shown in the amplified spectrum.

(E_C-E_F), and/or by modifying surface electric dipoles that control the difference between the vacuum level and the conduction band bottom, *i.e.*, the electron affinity $\chi = E_{vac} - E_C$. Thus, the work function can be expressed as the sum of two terms

$$WF = \chi + (E_C - E_F). \tag{11}$$

For a fixed value of the electron affinity, any shift in the position of the Fermi level with respect to the conduction band will result in an equal and opposite change of the work function. However, the electron affinity can be modified by gas treatments. Indeed, large changes in electron affinity (of about 1 eV) have been attributed to surface termination after oxidizing or reducing annealing.[27]

Photoelectron spectroscopies offer a direct manner to determine work functions. Indeed, the secondary electron onset provides a straight measurement of the specimen's work function. Then, with the help of this technique, we can investigate the influence on the work function of the treatments under oxygen and hydrogen. The results of the measurements are shown in Fig. 12. The derived work functions are 4.1 eV and 3.4 eV for S_{O2} and S_{H2} samples, respectively. A reduction in the work function, 0.7 eV in the present case, would be expected after the action of a reducing gas. At odds with Ref. 33, we found that this is not due to a change in the band bending, as derived from the results of Fig. 6, but from a change in the electron affinity.

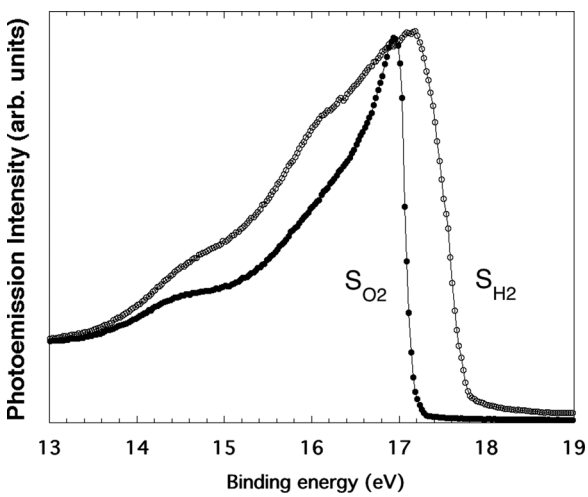

FIG. 12. Normalized secondary electron cutoff for the S_{H2} and S_{O2} samples. As observed, the exposure to hydrogen reduces the work function by 0.7 eV. Interestingly, this is not a consequence of changes in band bending but due to changes in the electron affinity.

IV. CONCLUSIONS

Gas detection with metal oxide is based on the presence of intergranular barriers that are modified with the exposure to different gaseous species. Thus, it is crucial to determine the basic mechanisms that alter those barriers responsible for the film conductivity. In this paper, we showed that polycrystalline tin oxide films present intergranular barriers that can be affected by thermal treatments at moderate temperatures. Interestingly, XPS results show that samples with different conductivities can present similar barrier heights. Thus, a thermionic mechanism cannot be responsible for the observed differences. Experiments indicate that oxygen diffusion into and out of the grains can change the doping to the point that they can present fully developed Schottky barriers, with quasi-neutral regions at their centers, or be completely depleted of carriers. In this paper, we specially focused on capacitance values, which were analyzed in detail considering the geometry involved to quantify doping changes due to in- and out-diffusion that leads to barriers overlapping. Also, we presented UPS results that show that exposing the SnO_2 samples to oxidizing or reducing environments modify the work function without modifying the band bending.

ACKNOWLEDGMENTS

This work was partially supported by the National Council for Scientific and Technical Research (CONICET) of Argentina and the National University of Mar del Plata (Argentina). We thank Daniel Mirabella for stimulating discussions.

[1]M. J. Madou and R. Morrison, *Chemical Sensing with Solid State Devices* (Academic, San Diego, 1989).
[2]N. Yamazoe, Sens. Actuators, B **108**, 2 (2005).
[3]N. Barsan, D. Koziej, and U. Weimar, Sens. Actuators, B **121**, 18 (2007).
[4]N. Barsan and U. Weimar, J. Electroceram. **7**, 143 (2001).
[5]K. Kao, *Dielectric Phenomena in Solids* (Elsevier Academic Press, San Diego, 2004).
[6]G. Blatter and F. Greuter, Phys. Rev. B **33**, 3952 (1986).
[7]M. A. Ponce, M. S. Castro, and C. M. Aldao, J. Mater. Sci.: Mater. Electron. **20**, 25 (2009).
[8]W. Gopel and K. Schierbaum, Sens. Actuators, B **26**, 1 (1995).
[9]V. P. B. Marques, A. Ries, A. Z. Simoes, M. A. Ramírez, J. A. Varela, and E. Longo, Ceram. Int. **33**, 1187 (2007).
[10]M. A. Ramírez, W. Bassi, R. Parra, P. R. Bueno, E. Longo, and J. A. Varela, J. Am. Ceram. Soc. **91**, 2402 (2008).
[11]M. A. Ramírez, W. Bassi, P. R. Bueno, E. Longo, and J. A. Varela, J. Phys. D: Appl. Phys. **41**, 122002 (2008).
[12]M. A. Ramírez, A. Z. Simoes, P. R. Bueno, M. A. Márquez, M. O. Orlandi, and J. A. Varela, J. Mater. Sci. **41**, 6221 (2006).
[13]M. S. Castro and C. M. Aldao, Ceram. Int. **22**, 39 (1996).

[14]G. Blaustein, M. S. Castro, and C. M. Aldao, Sens. Actuators, B **55**, 33 (1999).
[15]M. A. Ponce, M. S. Castro, and C. M. Aldao, Mater. Sci. Eng., B **111**, 14 (2004).
[16]M. A. Ponce, C. M. Aldao, and M. S. Castro, Mater. Sci. Eng., B **123**, 130 (2005).
[17]M. A. Ponce, C. Malagu, M. C. Carotta, G. Martinelli, and C. M. Aldao, J. Appl. Phys. **104**, 054907 (2008).
[18]C. M. Aldao, D. A. Mirabella, M. A. Ponce, A. Giberti, and C. Malagù, J. Appl. Phys. **109**, 063723 (2011).
[19]N. Yamazoe, J. Fuchigami, M. Kishikawa, and T. Seiyama, Surf. Sci. **86**, 335 (1979).
[20]S. C. Chang, J. Vac. Sci. Technol. **17**, 366 (1980).
[21]C. M. Aldao, F. Schipani, M. A. Ponce, E. Joanni, and F. J. Williams, Sens. Actuators, B **193**, 428 (2014).
[22]M. Kwoka, L. Ottaviano, M. Passacantando, S. Santucci, G. Czempik, and J. Szuber, Thin Solid Films **490**, 36 (2005).
[23]Zhi-Wen Chen, Chan-Hung Shek, C. M. Lawrence Wu, and J. K. L. Lai, Front. Mater. Sci. **7**, 203 (2013).
[24]C. Belmont and H. H. Gtrault, J. Appl. Electrochem. **24**, 475 (1994).
[25]D. Pascal, P. Dansas, C. Bru, and S. Laval, Semicond. Sci. Technol. **4**, 633 (1989).
[26]D. Gershon, J. P. Calame, and A. Birnboim, J. Appl. Phys. **89**, 8117 (2001).
[27]M. Batzill and U. Diebol, Prog. Surf. Sci. **79**, 47 (2005).
[28]O. Levy and D. Stroud, Phys. Rev. B **56**, 8035 (1997).
[29]M. S. Castro and C. M. Aldao, Appl. Phys. Lett. **63**, 1077 (1993).
[30]B. Kamp, R. Merkle, and J. Maier, Sens. Actuators, B **77**, 534 (2001).
[31]C. Malagù, A. Giberti, S. Morandi, and C. M. Aldao, J. Appl. Phys. **110**, 093711 (2011).
[32]M. A. Ponce, P. R. Bueno, J. Varela, M. S. Castro, and C. M. Aldao, J. Mater. Sci.: Mater. Electron. **19**, 1169 (2008).
[33]N. Barsan, M. Hübner, and U. Weimar, Sens. Actuators, B **157**, 510 (2011).